Available online at www.sciencedirect.com
ScienceDirect
Trans. Nonferrous Met. Soc. China 25(2015) 2458−2465
Transactions of Nonferrous Metals Society of China
www.tnmsc.cn

Electrodeposition behavior of bright nickel in air and water-stable betaine·HCl−ethylene glycol ionic liquid

Kai GONG[1,2], Yi-xin HUA[1,2], Cun-ying XU[1,2], Qi-bo ZHANG[1,2], Yan LI[1,2], Juan-jian RU[1,2], Ya-fei JIE[1,2]

1. Faculty of Metallurgical and Energy Engineering, Kunming University of Science and Technology, Kunming 650093, China;
2. State Key Laboratory of Complex Nonferrous Metal Resources Clean Utilization, Kunming 650093, China

Received 13 September 2014; accepted 13 May 2015

Abstract: The electrodeposition behaviors of nickel on glassy carbon (GC) and carbon steel (CS) electrodes were investigated in the 14.3%−85.7% (mole fraction) betaine·HCl−ethylene glycol (EG) ionic liquid using cyclic voltammetry and chronoamperometry. The results indicated that the reduction of Ni(II) on CS electrode via a diffusion-controlled quasi-reversible process was much more facile and easier than that occurred on GC electrode, which followed a diffusion-controlled three-dimensional instantaneous nucleation and growth. Scanning electron microscopy was used to observe that the deposit was dense and contained fine crystallites with average size of (80±4) nm. Energy dispersive spectrometer analysis showed that the obtained deposit was metallic nickel. X-ray diffraction spectroscopy indicated that (111) plane was the most preferred crystal orientation. The nickel deposit was luminous and bright, and had good adhesion with the CS substrate.

Key words: electrodeposition; bright nickel; nucleation mechanism; betaine·HCl; ethylene glycol

1 Introduction

Nickel and its alloys [1,2], such as Ni−Co [3,4], Ni−Fe [5,6], Ni−Cu [7], Ni−Zn [8], Ni−Al [9,10] and Ni−W [11,12] are most commonly used as anti-corrosion, decoration, heat-resistance and wear-resistant coatings. In addition, they have received considerable attention due to their commercial applications in various industrial fields [2,13−16]. While in the past few decades, the electrodeposition of nickel and its alloys has been widely attempted from a large amount of aqueous solutions, such as chloride, sulfate, sulfamate and Watts-type solutions [4,17]. In these conventional nickel-plating systems, hydrogen evolution often occurs during electrodeposition process, which results in profound effect on current efficiency and quality of the nickel deposits. To counteract these problems and achieve excellent coatings, some aprotic ionic liquids (ILs) are expected to be an ideal electrolyte for electrodeposition of nickel and its alloys. This type of ionic liquids usually provide a wide working potential and temperature range, acceptable conductivity and negligible vapor pressure (up to 300 °C) which is used as electrolytes/solutions without the occurring of hydrogen evolution [18,19].

Among the families of ionic liquids, room-temperature ionic liquids (RTILs)/deep eutectic solvents (DES) represent a series of solvents that have attracted intensive interests for electrodeposition of pure metals and metal alloys and other applications described in Refs. [20−25]. GALE et al [26] studied the equilibrium of the Ni(II) ions in chloroaluminate solvent by electrochemical and spectral measurements. They found that the reduction of the Ni(II) ion species on vitreous carbon electrodes exhibited irreversible behavior in acidic melts, but no $NiCl_4^{2-}$ ion reduction was detected in the basic solvent. Since chloroaluminate ionic liquids must be prepared and handled under an inert-gas atmosphere, DENG et al [27] successfully demonstrated the electrodeposition of Al, Mn, Ni, Zn, Sn, and Cu in the 1-methyl-3-alkylimidazolium or N-methyl-N-alkylpyrrolidinium cations with dicyanamide (DCA) anions. Nevertheless, such DCA-based ionic liquids are expensive. ABBOTT et al [20,28−32] and

Foundation item: Projects (51274108, 21263007, 51204080) supported by the National Natural Science Foundation of China; Project (2011FA009) supported by the Applied Research Foundation of Yunnan Province, China; Project (14118441) supported by the Talents Cultivation Foundation of Kunming University of Science and Technology, China
Corresponding author: Yi-xin HUA; Tel: +86-871-65162008; Fax: +86-871-65161278; E-mail: huakust@163.com
DOI: 10.1016/S1003-6326(15)63862-6

JAYAKUMAR et al [33] systematically expounded the concept of DES and investigated the properties of choline chloride-based eutectic melts as well as its applications in electrodeposition. However, so far at least as we are acquainted, the studies on the electrodeposition of nickel and nickel alloys in other air and water-stable RTILs (such as betaine hydrochloride-based ionic liquid) are very raw.

In this work, the 14.3%−85.7% (mole fraction) betaine·HCl−ethylene glycol (EG) ionic liquid (IL), due to its advantages such as being relatively benign, nontoxic and inexpensive and capable of large-scale processes, was used as the electrolyte for nickel deposition. Here, the purpose of this work is to preliminarily study the electrochemical behaviors and the electrodeposition of Ni(II) on both GC and CS electrodes in the 14.3%−85.7% betaine·HCl−EG IL. The elemental composition and surface morphology of the deposit were confirmed by X-ray diffraction (XRD) and scanning electron microscopy (SEM) coupled with energy dispersive analysis (EDS).

2 Experimental

2.1 Reagents

All chemical reagents used were analytically pure. Betaine·HCl (Hangzhou Wanjing New Material Co., Ltd, ≥98%) was dried under vacuum at 408 K for 16 h. Ethylene glycol (Xilong Chemical Co., Ltd, ≥99.9%) was pretreated by drying under vacuum at 353 K for 12 h. The mixture (the molar ratio was 1:6 for betaine·HCl to EG) was melted at 358 K in an oil bath thermostat under atmospheric condition, then dried under vacuum at 363 K for 24 h. Anhydrous nickel chloride was obtained by the dehydration of hexahydrated nickel chloride (Tianjin Fengchuan Chemical Reagent Technologies Co., Ltd, ≥98%) under vacuum at 418 K for 24 h. Then, a certain amount of anhydrous nickel chloride was dissolved into the neat melt at 353 K for less than 2 h to prepare the plating bath. The resulting solvent was an emerald green and clear liquid at room temperature.

2.2 Electrochemical measurements

Electrochemical measurements were performed using a CHI760D electrochemical workstation and based on the analysis of cyclic voltammetry and chronoamperometric current−time transients. A conventional three-electrode electrochemical cell was used at 358 K in an oil bath under atmospheric condition for these experiments. A silver wire (1 mm in diameter, and 10 mm in length) placed in a fritted porous glass tube containing the pure solvent was used as a quasi-reference electrode (QRE). All the potentials in this work were represented with this Ag-QRE. A GC electrode (d4 mm) and a CS electrode (0.42 cm^2 in effective dimension) were employed as the working electrode, respectively. Before each experiment, the working electrode was polished with 1200 grit silicon carbide papers and 0.5 μm high-purity alumina, rinsed with distilled water twice and finally dried. The chemical components of carbon steel (CS) electrode and CS substrate used are listed in Table1.

Table 1 Chemical components of CS electrode and CS substrate (mass fraction, %)

Fe	C	O	Si	P	S	Cr	Mn
96.905	0.835	1.405	0.085	0.058	0.095	0.180	0.440

For voltammetric experiments, a platinum wire (1 mm in diameter, and 10 mm in length) was used as a counter electrode. For electrodeposition experiments, nickel sheet (active area: 3 cm^2) was directly immersed in the solvent as the counter electrode in order to compensate for the consumption of Ni(II) species. Before each electrochemical deposition, the entire electrode surface was pretreated with aqua-regia at ambient temperature for 15−20 s, followed by polishing with 1200 grit silicon carbide papers, rinsing with running water and distilled water and air drying. After electrodeposition, the nickel deposit was cooled in air, washed with absolute ethanol to remove the melt residue, and rinsed with deionized water.

The surface morphology of the electrodeposited sample was characterized by using a Dutch Philips XL30 ESEM TMP model microscope. The preferred crystal orientation of the deposits was determined by using a Rigaku D/max-TTRIII X-ray diffractometer and compared with the standard copper ASTM data.

3 Results and discussion

3.1 Voltammetric analysis

Cyclic voltammograms (CVs) recorded on GC electrode for the 14.3%−85.7% (mole fraction) betaine·HCl−EG IL and its solution containing 0.137 mol/L $NiCl_2$ at 358 K with the scan rate of 30 mV/s are demonstrated in Fig. 1.

In the potential scan region, no apparent oxidation peak and reduction peak are observed (Fig. 1(a)). It can be concluded that the 14.3%−85.7% betaine·HCl−EG IL exhibits an electrochemical window of about 2.2 V. In contrast to Fig. 1(a), only one redox couple appears (Fig. 1(b)), proving this 14.3%−85.7% betaine·HCl−EG IL is available for nickel electrodeposition. The cathodic and anodic peaks are separated by near 1.04 V, indicating that the reduction of Ni(II) on GC electrode proceeds via a one-step two electrons transfer process and displays quasi-reversible behavior similar to Refs. [18,37], which

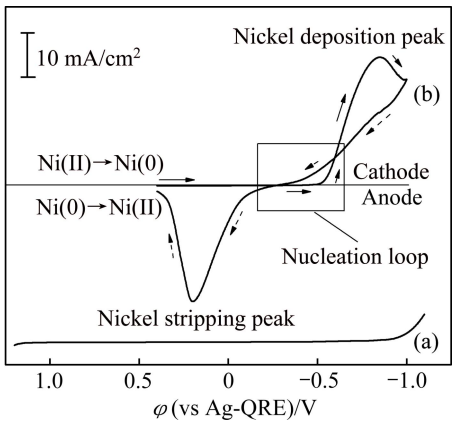

Fig. 1 Comparison of CVs recorded on GC electrode for neat 14.3%−85.7% betaine·HCl-EG IL (a) and its solution containing 0.137 mol/L $NiCl_2$ (b) at 358 K with scan rate of 30 mV/s

can be described by

$$Ni(II)+2e \rightarrow Ni(0) \quad (1)$$

As shown in Fig. 1(b), in the potential scan region, a prominent reduction wave is observed at −0.84 V due to the reduction of Ni(II) to Ni(0), and a corresponding oxidation wave is observed at around 0.2 V. By reversing, it exhibits an obvious nucleation loop [16] associated with this Ni(II)/Ni(0) redox couple (Fig. 1(b)), indicating that the nucleation and growth process of the nickel deposition on GC electrode requires overpotential to drive.

For further studies, Fig. 2 presents the comparison of CVs recorded on GC and CS electrodes as a function of scan rate at 358 K. The cathodic peak current increases and the cathodic peak potential shifts negatively with the increase of scan rate. As shown in Fig. 3(b), a good linear correlation is observed between the cathodic peak current density (J_{CP}) and the square root of the scan rate ($v^{1/2}$), suggesting that the reduction of Ni(II) on GC and CS electrodes is controlled by diffusion. The value of $|\varphi_{CP}-\varphi_{CP/2}|$ is larger than that required for a reversible process (57 mV at 303 K), proving that the reduction of Ni(II) on GC electrode is a quasi-reversible process [34−36]. All these characteristics indicate that the reduction of Ni(II) to Ni(0) on GC electrode is a diffusion-controlled quasi-reversible process.

Considering that the oxidation of iron occurs at a potential near that of nickel, the anodic potential scanning terminates before the stripping wave could occur. In contrast to the results obtained on GC electrode, the voltammograms recorded on CS electrode (Fig. 2(b)) exhibit no nucleation loop by reversing the sweep, implying that the nucleation/growth process of nickel on CS electrode is much more facile than that on GC electrode. It is observed that the cathodic peak

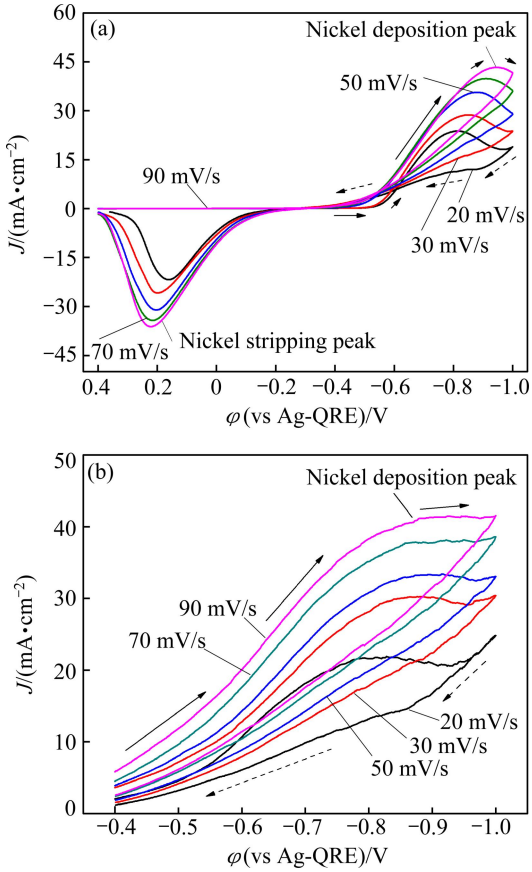

Fig. 2 Comparison of CVs recorded on GC electrode (a) and CS electrode (b) for reduction of Ni(II) (0.137 mol/L) in 14.3%−85.7% betaine·HCl-EG IL at 358 K as function of scan rate

current increases and the cathodic peak potential negatively shifts with increasing scan rate. The value of $|\varphi_{CP}-\varphi_{CP/2}|$ increases as the scan rate is increased. Similarly, the plots of J_{CP} against $v^{1/2}$ exhibit good linearity in accordance with CVs (Fig. 3(b)), which infers that the electrodeposition of nickel is controlled by diffusion process. These results suggest that reduction of Ni(II) to Ni(0) on CS electrode is also a diffusion-controlled quasi-reversible process.

For a quasi-reversible reduction reaction, the transfer coefficient can be calculated according to Eq. (2) which is usually used for irreversible cases [33−35]:

$$\left|\varphi_{CP}-\varphi_{CP/2}\right| = \frac{1.857RT}{\alpha n_\alpha F} \quad (2)$$

where R, T, φ_{CP}, $\varphi_{CP/2}$, α, n_α and F stand for mole gas constant, thermodynamic temperature, cathodic peak potential, cathodic half peak potential, transfer coefficient, the number of electrons transferred in the rate determining step, and Faraday constant, respectively.

According to the slope of the φ_{CP} vs ln v obtained from Fig. 3(a) and Eq. (2), the average values of αn_α are calculated to be 0.50 and 0.74 at 358 K for CS and GC electrodes, respectively.

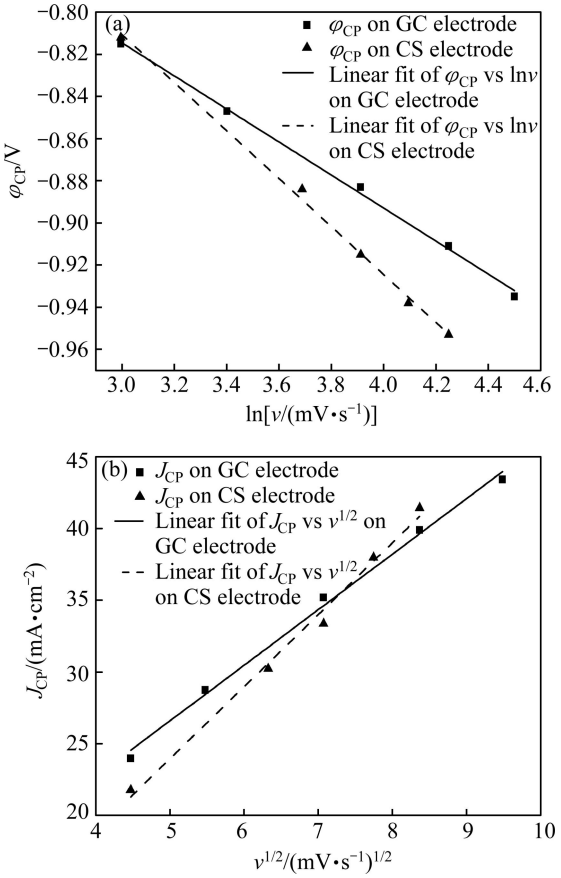

Fig. 3 Linear correlations between deposition peak potential (φ_{CP}) and ln v (a) and between cathode peak current J_{CP} and square root of scan rate $v^{1/2}$ (b)

The slope of the linear dependence of the cathode peak current on the square root of the potential sweep rate, shown in Fig. 3(b), could be used to calculate the diffusion coefficient of Ni(II) by applying the Randles–Sevcik equation [34−36]:

$$J_{CP} = 0.4958nFAC\left(\frac{\alpha n_\alpha FDv}{RT}\right)^{1/2} \quad (3)$$

where n, A, D and c mean the electron transfer number, electrode area, diffusion coefficient and bulk concentration of Ni(II), respectively.

According to Eq. (3), with the values of αn_α obtained from Eq. (2) and the slopes of the lines in Fig. 3(b), the diffusion coefficients of Ni(II) in the 14.3%−85.7% betaine·HCl−EG IL containing 0.137 mol/L $NiCl_2$ are calculated to be 2.87×10^{-6} cm^2/s and 2.31×10^{-6} cm^2/s at 358 K on CS and GC electrodes, respectively. The D-values are much larger than 4.40×10^{-8} cm^2/s at 353 K obtained in Ref. [37], which is far better for the diffusion of Ni(II) at the interface between electrode and solvent.

3.2 Nucleation and growth of nickel

To investigate the mechanism of nickel nucleation/growth process in more details, chronoamperometry experiments were performed. These experiments were carried out by negatively stepping the potentials that are sufficient to initiate a nucleation/growth process. Typical current−time transients resulting from these experiments are shown in Fig. 4. The Faradic current firstly increases due to the nucleation and growth of nickel nuclei and this rising current reaches the maximum, I_m, at time t_m, which is attributed to the three-dimensional growth of a nickel metal over the nuclei resulting in the increase of the surface area. Then, the current starts to decay due to the increase in diffusion layer thickness after reaching the maximum value. I_m increases while t_m shortens with increasing the applied nucleation overpotential.

Among the models for the nucleation and growth of crystals on the heterogeneous surface, a convenient method for identifying the nucleation mechanism was proposed by SCHARIFKER and HILLS [38]. Such model is represented by the following equations for instantaneous (Eq. (4)) and progressive (Eq. (5)) nucleation:

$$(I_{inst}/I_m)^2 = 1.9542\cdot \{[1-\exp(-1.2564t/t_m)]\}^2\times(t/t_m)^{-1} \quad (4)$$

$$(I_{prog}/I_m)^2 = 1.2254\cdot \{1-\exp[-2.3367(t/t_m)^2]\}^2\cdot(t/t_m)^{-1} \quad (5)$$

To determine the nucleation behavior, the experimental data are first normalized to I/I_m and t/t_m. Then, the normalized experimental data from the entire experimental current density−time transients resulting plots are compared with the theoretical dimensionless current density−time transients derived for instantaneous and progressive nucleation/growth models. These experimental and theoretical plots of $(I/I_m)^2$ against (t/t_m) are shown in Figs. 4(a′) and (b′). Moreover, it is apparently seen that the reduction of Ni(II) on GC electrode corresponds to a three-dimensional instantaneous nucleation/growth process.

The above-mentioned method proposed by SCHARIFKER and HILLS [38] was used to examine the experimental data, the rising current has a good linear relation with $t^{1/2}$ for the instantaneous nucleation of three-dimensional nuclei and $t^{3/2}$ for the progressive nucleation. The plots of J against $t^{1/2}$ (Fig. 5(a)) show a good linearity, further identifying that the electrodeposition of nickel on GC electrode follows a three-dimensional instantaneous nucleation and growth model. As shown in Fig. 5(b), the decrease of J has a good linear relation with $t^{-1/2}$, indicating that the growth of nickel nuclei on GC electrode follows a typical diffusion-controlled process. Thus, the reduction of Ni (II) on GC electrode follows a diffusion-controlled three-dimensional instantaneous nucleation/growth process.

Figure 4(b) shows that J decreases as time goes on.

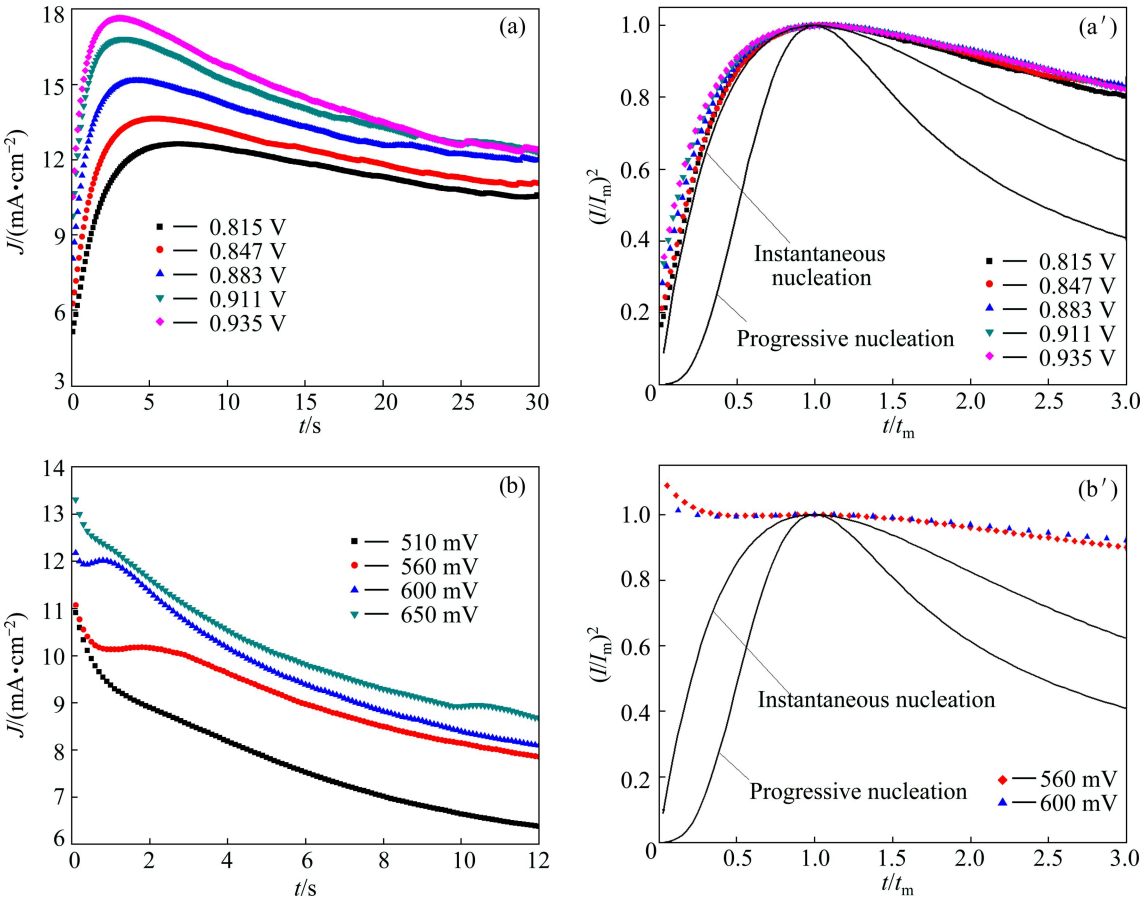

Fig. 4 Current−time transients of chronoamperometric experiments for reduction of Ni(II) on GC (a) and CS (b) electrodes in 14.3%−85.7% betaine·HCl−EG IL containing 0.137 mol/L $NiCl_2$ at 358 K (a′, b′) corresponding to (a) and (b), showing comparison of dimensionless experimental curves derived from current−time curves with theoretical models for 3D nucleation/growth process, respectively)

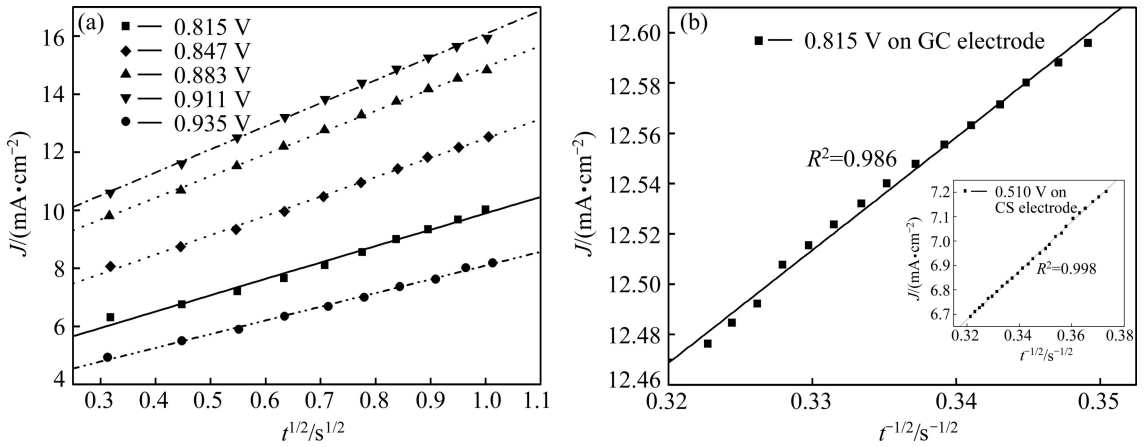

Fig. 5 Plot of J vs $t^{1/2}$ from rising portion of current−time transients recorded on CS electrode (a) and plot of J vs $t^{-1/2}$ from decreasing portion of current−time transients recorded on GC electrode (b) (Inset is a plot of J vs $t^{-1/2}$ from decreasing portion of current−time transients recorded on CS electrode)

From Fig. 4(b′), the experimental transients deviate a lot from the plots of theoretical models for 3D nucleation/growth process, illustrating that the model proposed by SCHARIFKER and HILLS [38] is not available for the reduction of Ni(II) on CS electrode. In view of the absence of current loop (Fig. 2(b)), the growth of nickel nuclei on CS electrode becomes much easier than that on CS electrode. In addition, as shown in

the inset of Fig. 5(b), the decrease of J has a good linear relationship with $t^{-1/2}$, indicating that the growth of nickel nuclei on CS electrode follows a typical diffusion-controlled process, which is consistent with the analysis of voltammetric measurements. The mechanism of the nickel nucleation/growth process on CS electrode will be discussed in more details in the further research.

3.3 Electrodeposition and characterization of nickel

Figure 6 shows the typical different magnified SEM micrographs of the surface morphology of the deposit prepared on CS substrate in the 14.3%−85.7% betaine·HCl−EG IL containing 0.137 mol/L $NiCl_2$ at 358 K with an applied cell voltage of 0.6 V for 3 h. It clearly reveals that the surface morphologies of the deposit are smooth, compact and dense. In addition, the deposit obtained on the surface of CS substrate by potentiostatic method consists of homogeneous grains with the average size of about (80±4) nm.

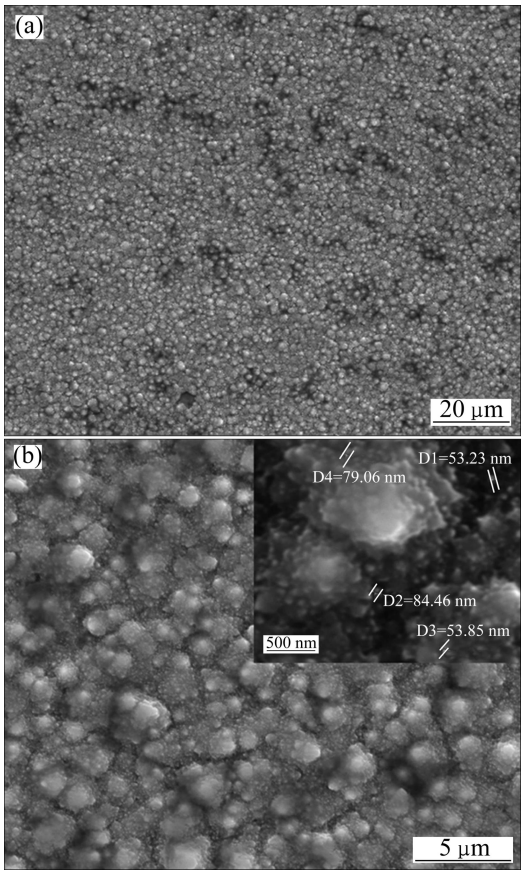

Fig. 6 Typical different magnified SEM micrographs of deposit prepared on CS substrate with applied cell voltage of 0.6 V in 14.3%−85.7% betaine·HCl−EG IL containing 0.137 mol/L $NiCl_2$ at 358 K for 3 h

Figure 7(a) shows the accompanying EDS spectrum of the deposit. It clearly reveals only the trace of nickel element exists, indicating that no ionic liquid residue is trapped in the deposit and the deposit is metallic nickel. Figure 7(b) illustrates the XRD pattern of nickel deposit, from which it is seen that the diffraction peaks of nickel deposit are consistent with face-center-cubic structure. The nickel deposit exhibits four clear diffraction peaks of (111), (200), (220) and (311) with (111) as the most preferred orientation. According to XRD analysis, using the Scherrer formula (d=0.9λ/(βcosθ), where λ is the X-ray wavelength, θ is the diffraction angle and β is the half width at half height for the diffraction peak in radians), average sizes of crystallites were around between 17 and 73 nm.

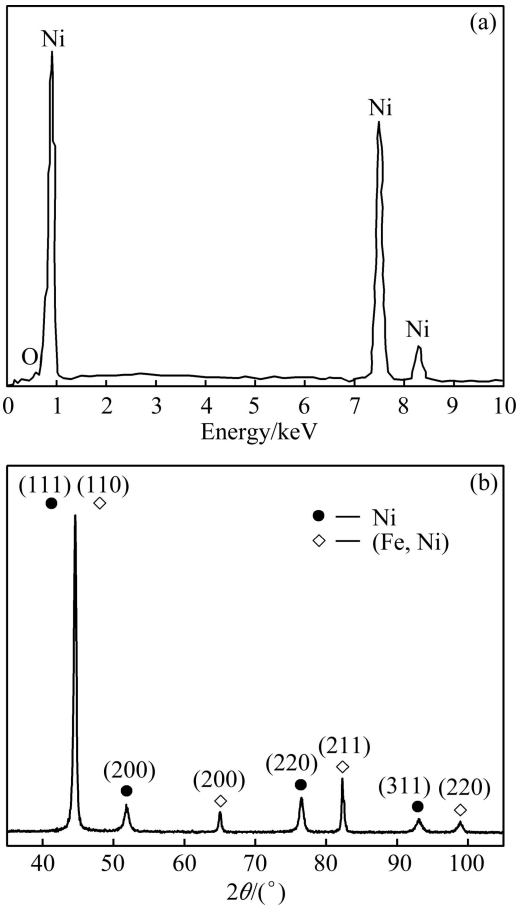

Fig. 7 EDS (a) and XRD pattern (b) analyses for nickel deposit obtained on CS substrate at given cell voltage of 0.6 V in 14.3%−85.7% betaine·HCl-EG IL containing 0.137 mol/L $NiCl_2$ at 358 K for 3 h

Figures 8(a) and (b) respectively show the digital and metallographic section images of the nickel deposit prepared on CS substrate at the given cell voltage of 0.6 V in the 14.3%−85.7% betaine·HCl-EG IL containing 0.137 mol/L $NiCl_2$ at 358 K for 3 h. It is obviously seen that the nickel deposit with a thickness of 19.53 μm is very luminous and bright, and has good adhesion with the CS substrate, indicating that bright nickel coating on CS substrate could be directly obtained in the 14.3%−85.7% betaine·HCl−EG IL without any additive.

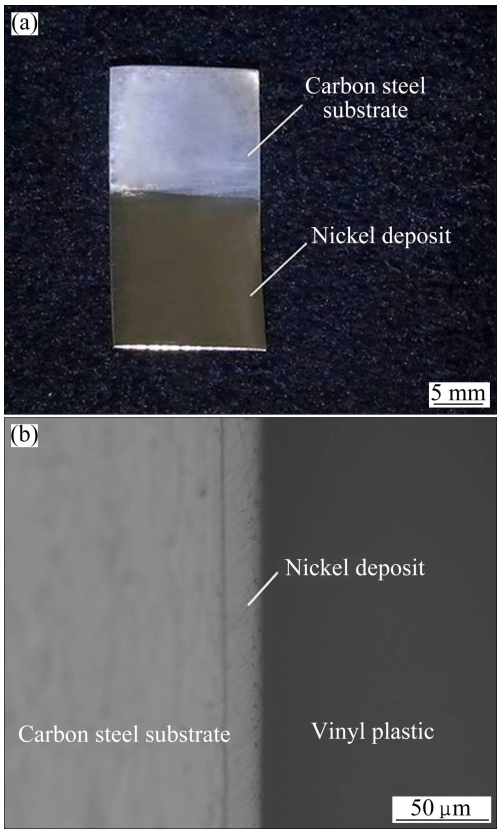

Fig. 8 Digital (a) and metallographic section (b) images of nickel deposit prepared on CS substrate at given cell voltage of 0.6 V in 14.3%−85.7% betaine·HCl-EG IL containing 0.137 mol/L $NiCl_2$ at 358 K for 3 h

4 Conclusions

1) Cyclic voltammetric studies reveal that the reduction of Ni(II) to Ni(0) on GC and CS electrodes is associated with a diffusion-controlled quasi-reversible nucleation/growth process. The average values of αn_α are calculated to be 0.50 and 0.74 with the corresponding diffusion coefficients of Ni(II) to be 2.87×10^{-6} and 2.31×10^{-6} cm^2/s at 358 K on CS and GC electrodes, respectively.

2) Chronoamperometric analysis indicates that the electroreduction of Ni(II) on GC electrode is a diffusion-controlled three-dimensional instantaneous nucleation and growth process. In contrast to the results obtained on GC electrode, the nucleation and growth of nickel on CS electrode becomes much easier and more facile, following a diffusion-controlled nucleation process.

3) Bright nickel deposit with the thickness of 19.53 μm can be directly obtained on CS substrate in the 14.3%−85.7% betaine·HCl−EG IL without any additive. The deposit is bright, uniform and dense, which shows excellent adhesion with CS substrate with round crystallites in the nanometer size regime.

Acknowledgements

The authors would like to thank Dr. ZHOU Lie-xing in Analytic & Testing Research Center of Yunnan Province, China for assistance with the SEM analysis.

References

[1] FLOREA A, ANICAI L, COSTOVICI S, GOLGOVICI F, VISAN T. Ni and Ni alloy coatings electrodeposited from choline chloride-based ionic liquids-electrochemical synthesis and characterization [J]. Surface and Interface Analysis, 2010, 42(6−7): 1271−1275.

[2] ORIŇÁKOVÁ R, TUROŇOVÁ A, KLADEKOVÁ D, GALOVÁ M, SMITH R M. Recent developments in the electrodeposition of nickel and some nickel-based alloys [J]. Journal of Applied Electrochemistry, 2006, 36(9): 957−972.

[3] YOU Yi-hui, GU Chang-dong, WANG Xiu-li, TU Jiang-ping. Electrodeposition of Ni−Co alloys from a deep eutectic solvent [J]. Surface and Coatings Technology, 2012, 206(17): 3632−3638.

[4] GOLODNITSKY D V, GUDIN N A, VOLYANUK G. Study of nickel−cobalt alloy electrodeposition from a sulfamate electrolyte with different anion additives [J]. Journal of the Electrochemical Society, 2000, 147(11): 4156−4163.

[5] SAM S, FORTAS G, GUITTOUM A, GABOUZE N, DJEBBAR S. Electrodeposition of NiFe films on Si (100) substrate [J]. Surface Science, 2007, 601(18): 4270−4273.

[6] MCCREA J L, PALUMBO G, HIBBARD G D, ERB U. Properties and applications for electrodeposited nanocrystalline Fe−Ni alloys [J]. Reviews on Advanced Materials Science, 2003, 5(3): 252−258.

[7] WANG Shao-hua, GUO Xing-wu, YANG Hai-yan, DAI Ji-chun, ZHU Rong-yu, GONG Jia, PENG Li-ming, DING Wen-jiang. Electrodeposition mechanism and characterization of Ni−Cu alloy coatings from a eutectic-based ionic liquid [J]. Applied Surface Science, 2014, 288: 530−536.

[8] YANG Hai-yan, GUO Xing-wu, CHEN Xiao-bo, WANG Shao-hua, WU Guo-hua, DING Wen-jiang. On the electrodeposition of nickel–zinc alloys from a eutectic-based ionic liquid [J]. Electrochimica Acta, 2012, 63: 131−138.

[9] PITNER W R, HUSSEY C L, STAFFORD G R. Electrodeposition of nickel−aluminum alloys from the aluminum chloride-1-methyl-3-ethylimidazolium chloride room temperature molten salt [J]. Journal of the Electrochemical Society, 1996, 143(1): 130−138.

[10] ALI M R, NISHIKATA A, TSURU T. Electrodeposition of Al−Ni intermetallic compounds from aluminum chloride-N-(n-butyl) pyridinium chloride room temperature molten salt [J]. Journal of Electroanalytical Chemistry, 2001, 513(2): 111−118.

[11] LEE D B, KO J H, KWON S C. High temperature oxidation of Ni−W coatings electroplated on steel [J]. Materials Science and Engineering A, 2004, 380(1): 73−78.

[12] ALIMADADI H, AHMADI M, ALIOFKHAZRAEI M, YOUNESI R. Corrosion properties of electrodeposited nanocrystalline and amorphous patterned Ni−W alloy [J]. Materials & Design, 2009, 30(4): 1356−1361.

[13] LANDOLT D. Electrodeposition science and technology in the last quarter of the twentieth century [J]. Journal of the Electrochemical Society, 2002, 149(S3): s9−s20.

[14] PARK J Y, ALLEN M G. Development of magnetic materials and processing techniques applicable to integrated micromagnetic devices [J]. Journal of Micromechanics & Microengineering, 1998, 8(4): 307−316.

[15] MANN O, PAN G B, FREYLAND W. Nanoscale electrodeposition of metals and compound semiconductors from ionic liquids [J]. Electrochimica Acta, 2009, 54(9): 2487−2490.
[16] LI Jia-xin, LAI Heng, FAN Bi-jiang, ZHUANG Bin, GUAN Lun-hui, HUANG Zhi-gao. Electrodeposition of RE−TM (RE= La, Sm, Gd; TM= Fe, Co, Ni) films and magnetic properties in urea melt [J]. Journal of Alloys and Compounds, 2009, 477(1): 547−551.
[17] CISZEWSKI A, POSLUSZNY S, MILCZAREK G, BARANIAK M. Effects of saccharin and quaternary ammonium chlorides on the electrodeposition of nickel from a Watts-type electrolyte [J]. Surface & Coatings Technology, 2004, 183(2): 127−133.
[18] ENDRES F, MACFARLANE D, ABBOTT A. Electrodeposition from Ionic liquids [M]. Weinheim: John Wiley & Sons, 2008.
[19] OHNO H. Electrochemical aspects of ionic liquids [M]. 2nd ed. New York: John Wiley & Sons, 2011.
[20] ABBOTT A P, MCKENZIE K J. Application of ionic liquids to the electrodeposition of metals [J]. Physical Chemistry Chemical Physics, 2006, 8(37): 4265−4279.
[21] ENDRES F. Ionic liquids: Solvents for the electrodeposition of metals and semiconductors [J]. Chem Phys Chem, 2002, 3(2): 144−154.
[22] YAMAGATA M, TACHIKAWA N, KATAYAMA Y, MIURA T. Electrochemical behavior of several iron complexes in hydrophobic room-temperature ionic liquids [J]. Electrochimica Acta, 2007, 52(9): 3317−3322.
[23] FREYLAND W, ZELL C A, ABEDIN S, EI ABEDIN S Z, ENDRES F. Nanoscale electrodeposition of metals and semiconductors from ionic liquids [J]. Electrochimica Acta, 2003, 48(20): 3053−3061.
[24] ABBOTT A P, FRISCH G, HARTLEY J, RYDER K S. Processing of metals and metal oxides using ionic liquids [J]. Green Chemistry, 2011, 13(3): 471−481.
[25] SIMKA W, PUSZCZYK D, NAWRAT G. Electrodeposition of metals from non-aqueous solutions [J]. Electrochimica Acta, 2009, 54(23): 5307−5319.
[26] GALE R J, GILBERT B, OSTERYOUNG R A. Electrochemical and spectral investigations of nickel(II) ion equilibriums in room-temperature chloroaluminate solvents [J]. Inorganic Chemistry, 1979, 18(10): 2723−2725.
[27] DENG Ming-jia, CHEN Po-yu, LEONG Tin-lao, SUN I-wen, CHANG Jeng-kuei, TSAI Wen-ta. Dicyanamide anion based ionic liquids for electrodeposition of metals [J]. Electrochemistry Communications, 2008, 10(2): 213−216.
[28] ABBOTT A P, CAPPER G, DAVIES D L, RASHEED R K, TAMBYRAJAH V. Novel solvent properties of choline chloride/urea mixtures [J]. Chemical Communications, 2003 (1): 70−71.
[29] ABBOTT A P, CAPPER G, DAVIES D L, RASHEED R K. Ionic liquid analogues formed from hydrated metal salts [J]. Chemistry—A European Journal, 2004, 10(15): 3769−3774.
[30] ABBOTT A P, BOOTHBY D, CAPPER G, DAVIES D L, RASHEED R K. Deep eutectic solvents formed between choline chloride and carboxylic acids: Versatile alternatives to ionic liquids [J]. Journal of the American Chemical Society, 2004, 126(29): 9142−9147.
[31] ABBOTT A P, CAPPER G, DAVIES D L, RASHEED R K, SHIKOTRA P. Selective extraction of metals from mixed oxide matrixes using choline-based ionic liquids [J]. Inorganic Chemistry, 2005, 44(19): 6497−6499.
[32] ABBOTT A P, EI TTAIB K, RYDER K S, SMITH E L. Electrodeposition of nickel using eutectic based ionic liquids [J]. Transactions of the Institute of Metal Finishing, 2008, 86(4): 234−240.
[33] JAYAKUMAR M, VENKATESAN K A, SRINIVASAN T G. Electrochemical behavior of fission palladium in 1-butyl-3-methylimidazolium chloride [J]. Electrochimica Acta, 2007, 52(24): 7121−7127.
[34] BARD A J, FAULKNER L R. Electrochemical methods: Fundamentals and applications [M]. New York: Wiley, 1980.
[35] AKIRA G, MASUO A, INOUE W. Electrochemical measurement method [M]. CHEN Zhen, YAO Jian-nian, trans. Beijing: Beijing University Press, 1995: 156−158. (in Chinese)
[36] WANG Rui, HUA Yi-xin, ZhANG Qi-bo. Electrochemical preparation of copper nanoparticles in choline chloride-urea deep eutectic solvent [J]. ECS Transactions, 2014, 59(1): 505−511.
[37] LI M, WANG Z W, REDDY R G. Electrodeposition of nickel in 1-butyl-3-methylimidazolium tetrafluoroborate ionic liquids [J]. Journal of the Electrochemical Society, 2014, 161(4): D150−D153.
[38] SCHARIFKER B, HILLS G. Theoretical and experimental studies of multiple nucleation [J]. Electrochimica Acta, 1983, 28(7): 879−889.

光亮镍在甜菜碱盐酸盐−乙二醇离子液体中的电沉积行为

龚 凯[1,2]，华一新[1,2]，徐存英[1,2]，张启波[1,2]，李 艳[1,2]，汝娟坚[1,2]，介亚菲[1,2]

1. 昆明理工大学 冶金与能源工程学院，昆明 650093；
2. 复杂有色金属资源清洁利用国家重点实验室，昆明 650093

摘 要：采用循环伏安和计时电流法，在14.3%~85.7%(摩尔分数)的甜菜碱盐酸盐−乙二醇离子液体中研究镍在玻碳电极和碳钢电极上的电沉积行为。结果表明：相比Ni(II)在玻碳电极上受扩散控制的三维瞬时形核过程，Ni(II)在碳钢电极上受扩散控制的准可逆还原过程更容易。SEM和EDAX表明在碳钢片上电沉积得到的镀层为金属镍，且镀层致密、均匀，晶粒细小(平均粒径为(80±4) nm)。XRD表明，(111)晶面为镍在碳钢片上的最优生长晶面。镀层表面平整光亮，与碳钢基体有良好的附着力。

关键词：电沉积；光亮镍；形核机理；甜菜碱盐酸盐；乙二醇

(Edited by Xiang-qun LI)